# Elongated Metal Nanocap with Two Magnetic Dipole Resonances and Its Application for Upconversion Enhancement

Hinamoto, Tatsuki
Higashiura, Tomoki
Sugimoto, Hiroshi
Fujii, Minoru

(Citation)
The Journal of Physical Chemistry C,123(42):25809-25815

(Issue Date)
2019-10-04

(Resource Type)
journal article

(Version)
Accepted Manuscript

# Elongated Metal Nanocap with Two Magnetic Dipole Resonances and Its Application for Upconversion Enhancement

*Tatsuki Hinamoto, Tomoki Higashiura, Hiroshi Sugimoto, and Minoru Fujii**

Department of Electrical and Electronic Engineering, Graduate School of Engineering, Kobe University, Rokkodai, Nada, Kobe 657-8501, Japan

ABSTRACT. A stand-alone plasmonic nanocomposite into which a metal nanostructure and an emitting material are integrated is a promising building block for optoelectronics and biophotonics devices. Here we present the plasmonic property of a nanocomposite composed of a Au elongated nanocap and a β-$NaYF_4$ dielectric nanorod. We show that elongation of a Au nanocap results in splitting of the magnetic dipole resonance, and the resonance wavelengths can be controlled in a wide wavelength range by the aspect ratio. As an application of the elongated nanocap, we demonstrate strong enhancement of the near-infrared to visible upconversion of an $Er^{3+}$ and $Yb^{3+}$ doped β-$NaYF_4$ nanorod by tuning the resonance wavelength of a Au nanocap placed on it to the excitation wavelength.

## INTRODUCTION

Plasmonic nanostructures control electromagnetic field at the nanoscale and engineer the radiation property, *i.e.,* the radiation pattern, the quantum efficiency, and the excitation rate, of a coupled emitter such as a molecule, an ion and a quantum dot.[1–8] Among various kinds of plasmonic nanostructures, a stand-alone plasmonic nanocomposite, into which a metal nanostructure and an emitting material are integrated, has been attracting attention in different fields because it can be a functional building block in optoelectronics and biophotonics devices. A large variety of metal nanostructures have been employed for the formation of stand-alone plasmonic nanocomposites. They are nanoparticles[9–12], nanorods[13–17], nanoshells[18,19], nanomatryoshkas[20], core-shell nanorods[21,22], nanocaps[23–25], core-cap couples[26], nanoparticle dimers[27,28], metal-insulator-metal sandwichs[29], nanoparticle clusters[30,31], and nanorod clusters[32].

Prerequisite properties of metal nanostructures used in plasmonic nanocomposites are the existence of multiple resonances for the enhancement of both the excitation and emission processes of a coupled emitter, wide tunability of the resonance wavelengths, accessibility of an emitter to the hot spots, capability of the radiation pattern control, etc. A metal nanocap is one of the metal nanostructures having these properties. It possesses the magnetic dipole mode arising from circulating current along the cap surface in addition to the electric dipole mode; the resonance wavelengths can be controlled by the structural parameters.[33–37] Furthermore, it has a unique focusing property for the radiation of a coupled emitter.[24–26] The resonance wavelength of the magnetic dipole mode depends on the length of the current path. Therefore, introduction of anisotropy in the nanocap structure results in the splitting of the magnetic dipole mode, which further increases the flexibility of the radiation control property.

In this paper, we propose a metal nanocap being elongated to the direction perpendicular to the nanocap axis (elongated nanocap) as a novel platform for a plasmonic nanocomposite. First, through full-wave numerical simulation, we examine the spectral response of the elongated nanocap with various aspect ratios. We show that elongation of a nanocap to one direction lifts the degeneracy of the magnetic dipole mode and that the resonance wavelengths can be controlled in a wide wavelength range by the aspect ratio. We then develop a process for the fabrication of a nanocomposite composed of an $Er^{3+}$ and $Yb^{3+}$ doped hexagonal-phase $NaYF_4$ (β-$NaYF_4$) nanorod and an elongated nanocap made of Au. We demonstrate by single particle scattering measurements in combination with transmission electron microscope (TEM) observations that the surface plasmon resonance wavelengths can be controlled in a wide wavelength range as predicted by numerical simulations. Finally, we demonstrate strong enhancement of the near-infrared to visible upconversion of an $Er^{3+}$ and $Yb^{3+}$ doped β-$NaYF_4$ nanorod by tuning the resonance wavelength of a Au nanocap placed on it to the excitation wavelength.

## COMPUTATIONAL ANALYSIS

We performed the computational analysis of an elongated nanocap using a boundary element method (BEM).[38,39] The structure composed of an elongated Au nanocap and a β-$NaYF_4$ nanorod was modeled with a freely available modeling software Gmsh[40]. Figure 1a and b shows the simulation model of a β-$NaYF_4$ nanorod with an elongated nanocap. A β-$NaYF_4$ nanorod has a hexagonal cross-section; the dimension of the nanorod is defined by the length (long axis: L) and the diameter of the incircle (short axis: S). A nanocap covers the upper half of the nanorod. The outer surface of the nanocap is inscribed to an ellipse: the half-lengths of the major and minor axes

are $T + S/2 - S'/8$ and $T/4 + S'/2$, respectively, where $T$ and $S'$ are the thickness of the nanocap and the diameter of the circumcircle of the nanorod's hexagonal cross section, respectively. The edge of the nanocap is rounded. The dielectric function of Au is taken from a literature[41], while a constant value of 1.475[2] is used for β-$NaYF_4$. All simulations were performed in vacuum.

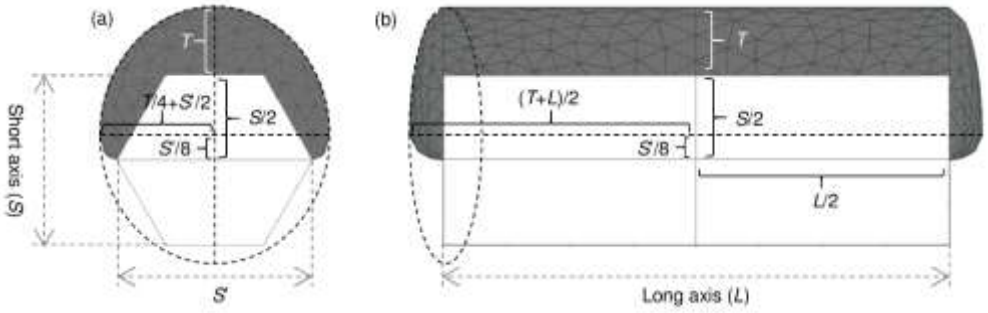


**Figure 1.** Simulation model of an elongated nanocap formed on a β-$NaYF_4$ dielectric nanorod. (a) front and (b) side view of the structure. The structure is defined by structural parameters: the length of the long axis ($L$) of the nanorod, the diameters of the incircle ($S$) and circumcircle ($S'$) of the hexagonal cross section of the nanorod, and the thickness of the nanocap ($T$).

Figure 2a and b show the extinction spectra of elongated nanocaps with the aspect ratios ($S/L$) of 1 and 4, respectively, and Figure 2c shows the color plot of extinction spectra as a function of wavelength and long axis length (*i.e.,* aspect ratio). The short axis length and the nanocap thickness are set to 50 nm and 20 nm, respectively, while the long axis length is changed from 50 nm to 200 nm. The spectra are obtained by averaging the spectra of 6 different illumination geometries, that is, the direction of propagation and polarization (**k**, **E**) are ($k_z$, $E_y$) (1-1), ($k_z$, $E_x$) (1-2), ($k_y$, $E_z$) (2-1), ($k_y$, $E_x$) (2-2), ($k_x$, $E_y$) (3-1), and ($k_x$, $E_z$) (3-2). When the aspect ratio is 1 (Figure 2a), the extinction spectrum is dominated by almost one resonance, which can be assigned to a magnetic dipole (MD) mode (transverse mode) arising from a current loop in the nanocap.[24,26,33–37] The small

splitting of the peak arises from the small anisotropy of the nanocap model even when the aspect ratio is 1 (see the illustration in the inset). A small peak at 554 nm is an electric dipole (ED) mode (axial mode). When the aspect ratio is 4, the splitting of the MD mode becomes large, and the long wavelength peak reaches around 1020 nm (Figure 2b). Figure 2c shows the color plot of extinction spectra as a function of wavelength and long axis length. The short axis length is fixed. We can see the increase of the splitting of the MD mode with increasing the aspect ratio. Hereafter, we denote the MD modes at short and long wavelengths as MD (S) and MD (L), respectively, because they arise from current loops along the long and short axes, respectively. The wavelength of the MD (S) mode is almost independent of the aspect ratio, while that of the MD (L) mode depends strongly on the ratio.

To gain more insight into the LSPR modes in elongated nanocaps, we show the extinction spectra in different excitation geometries in Figure 2d-i. The geometries are shown in the inset of each figure. The MD (L) mode is excited when the electric field of the excitation light is polarized along the long axis (Figure 2d and h), while the MD (S) mode is excited when the polarization is along to the short axis (1-2 and 2-2 geometries in Figure 2e and g). In 2-1 and 3-2 geometries (Figure 2f and i), the polarization is perpendicular to both the long and short axes. In these geometries, the ED mode (axial mode) is excited around 550 nm.[24,26,33–37] The ED mode is almost independent of the aspect ratio and is much weaker than the MD modes. Therefore, the contribution of the ED mode is very limited in Figure 2a and b.

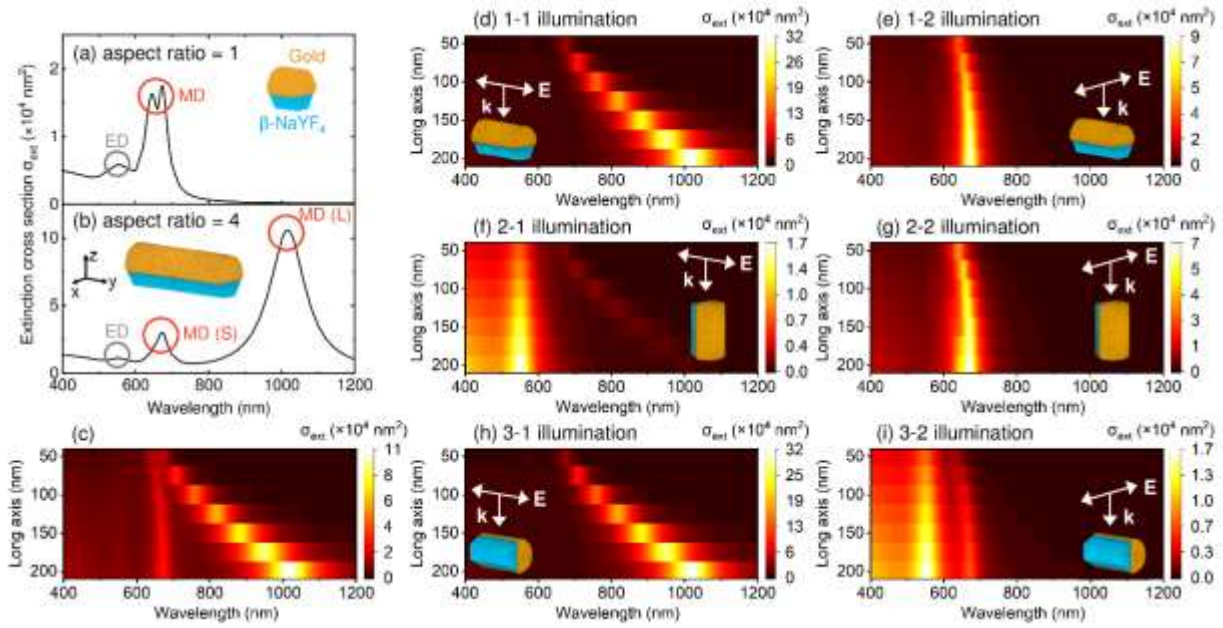


**Figure 2.** Simulated extinction spectra of elongated nanocap in free space. The short axis length is 50 nm and the nanocap thickness is 20 nm. The long axis length is changed from 50 nm to 200 nm. (a–b) Extinction spectra of nanocaps with the aspect ratios of 1 (long axis = 50 nm) (a) and 4 (long axis = 200 nm) (b). (c) Color plot of extinction spectra as a function of wavelength and long axis length (*i.e.,* aspect ratio). In (a-c), the spectra are obtained by averaging the spectra of 6 different illumination geometries shown in the insets of (d–i). (d–i) Color plots of extinction spectra as a function of wavelength and long axis length (*i.e.,* aspect ratio) for different illumination geometries; (d) 1-1, (e) 1-2, (f) 2-1, (g) 2-2, (h) 3-1, and (i) 3-2. Insets are schematic drawings of the illumination geometries.

Based on the information obtained from Figure 2, we deduce optimized structure to maximize upconversion of an $Er^{3+}$ and $Yb^{3+}$ doped β-$NaYF_4$ nanorod. In the system, $Er^{3+}$ absorbs 980 nm photons with a help of $Yb^{3+}$ ions and emits green (560 nm) and red (660 nm) photons via multi-step excitation processes. Therefore, large upconversion enhancement is expected if LSPR

resonances of a nanocap are brought to these wavelengths. Figure 3a shows the extinction spectrum of a structure satisfying the condition; the lengths of short and long axes of a β-$NaYF_4$ nanorod are 46 nm and 186 nm (aspect ratio≈4), respectively, and the thickness of a Au nanocap is 20 nm. The MD (L) mode is tuned to the excitation wavelength and the MD (S) mode is tuned to the red emission.

In order to quantitatively evaluate the upconversion enhancement, we first calculate the electric field distribution ($|\mathbf{E}/\mathbf{E_0}|$). Figure 3b and c show electric field distributions at 660 and 980 nm in the planes shown in the inset. In both cases, the electric fields are strongly enhanced in the whole volume of the β-$NaYF_4$ nanorod. The enhancement factors at the center of the nanorods are 7.8 and 5.8 for MD (S) and MD (L) modes, respectively.

We then calculate the antenna efficiency ($\eta_a$), which is defined by the ratio of the enhancement factor of the radiative decay rate ($\gamma_{radiative}$) to that of the total decay rate ($\gamma_{total}$).[6,42,43] Figure 3d shows the antenna efficiency spectrum obtained by averaging the calculated antenna efficiencies for point dipoles along x, y and z directions placed at the center of the nanorod. Similar to the extinction spectra, the antenna efficiency spectrum is dominated by two peaks, corresponding to the MD (S) and MD (L) modes. The antenna efficiency is around 30% at the red emission wavelength. This value is much larger than the quantum efficiency of $Er^{3+}$ and $Yb^{3+}$ doped β-$NaYF_4$ generally reported (typically ~1%)[44,45]. Therefore, we can expect roughly 10-fold enhancement of the quantum efficiency by the Purcell effect.

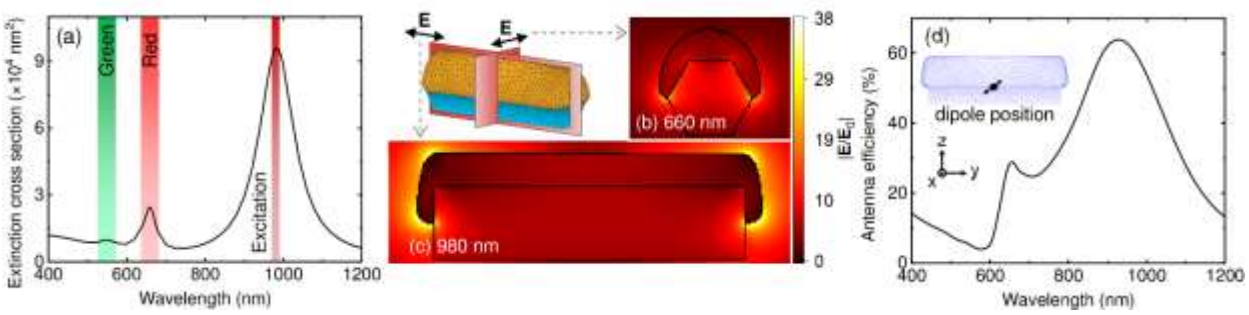

**Figure 3.** (a) Calculated extinction spectrum (averaged spectra of 6 different illumination geometries in Figure 2), (b,c) electric field distributions at 660 nm (b) and 980 nm (c), and (d) antenna efficiency of an $Er^{3+}$ and $Yb^{3+}$ doped β-$NaYF_4$ nanorod with a Au nanocap. The short axis length, the long axis length, and the nanocap thickness are 46 nm, 186 nm, and 20 nm, respectively. The structure is optimized to bring the MD (L) mode to the excitation wavelength (980 nm) and the MD (S) mode to the red emission wavelength (660 nm). The antenna efficiency is obtained by averaging the calculated antenna efficiencies for point dipoles along x, y and z directions placed at the center of the nanorod.

## EXPERIMENTAL METHODS

Figure 4 shows the fabrication procedure of an $Er^{3+}$ and $Yb^{3+}$ doped β-$NaYF_4$ (β-$NaYF_4$:Er/Yb) nanorod with an elongated Au nanocap. First, β-$NaYF_4$:Er/Yb nanorods with the aspect ratio of 1 to 4 were synthesized by a hydrothermal method (See Supporting Information for details).[46,47] Synthesized nanorods were placed on a glass slide by drop-casting the diluted suspension. Following the deposition of a titanium (Ti) adhesion layer (1 nm in thickness), Au (20 or 30 nm in thickness) was deposited on top of the nanorods by thermal evaporation with the deposition rate of 0.1 nm/s. The nanorods were isolated from the glass slide by ultrasonication in ethanol, and the solution was concentrated by centrifugation. Finally, the solution was dropped on a carbon-coated TEM mesh for TEM observations (JEM–2100F (JEOL), JED–2300T (JEOL) and H–7000 (Hitachi)). In TEM images, together with single nanorods with the structure similar to the model structure in Figures 1 and 2, dimers, trimers, agglomerates, nanorods with an Au nanocap on the side surface, etc. (Figure S1 in the Supporting Information) were observed. We recorded the positions of single isolated nanorods with the structure similar to the model structure in a TEM

mesh for the optical measurements. With this procedure, one-to-one correspondence of a TEM image and optical spectra becomes possible.

The TEM mesh was then transferred to a custom-built inverted optical microscope (Nikon) for the optical spectroscopy. For the measurement of scattering spectrum, a sample was epi-illuminated by a halogen lamp through a bright and dark field objective (100×/0.9 NA, LU Plan Fluor, Nikon) in dark-field geometry. In a scattering image, an individual nanorod, the position of which was recorded in advance by TEM observations, was selected by a pin-hole (200 μm in diameter) placed at the confocal plane of the microscope, and the image was sent to the entrance slit of a monochromator (iHR320, Horiba Jobin Yvon) equipped with a liquid-nitrogen-cooled charge coupled device (CCD) and an InGaAs diode array (Symphony, Horiba Jobin Yvon). The 200 μm pin-hole corresponds to 2 μm in the image plane. Following the measurement of the scattering spectrum, the upconversion spectrum of the same nanorod was measured by the same setup. For the upconversion measurement, the sample was epi-illuminated coaxially through the same objective by 975 nm light (1.1 kW/cm$^2$) from a semiconductor laser.

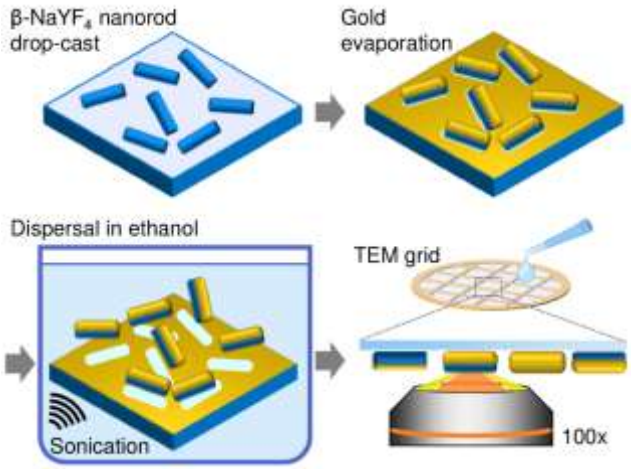


**Figure 4.** Schematic illustration of the fabrication procedure of the β-$NaYF_4$ nanorod with Au nanocap.

EXPERIMENTAL RESULTS AND DISCUSSION

Figure 5a-d show TEM images of synthesized β-$NaYF_4$:Er/Yb nanorods with different aspect ratios; the typical dimensions estimated from TEM images are 100 × 150 nm (aspect ratio 1.5), 100 × 200 nm (aspect ratio 2), 75 × 230 nm (aspect ratio 3), and 50 × 200 nm (aspect ratio 4), respectively. Figure 5e-h are the TEM image, the HAADF-STEM image, the EDS mapping image (Au and F), and the schematic illustration, respectively, of a β-$NaYF_4$:Er/Yb nanorod (105 × 177 nm) on which a Au nanocap (30 nm in thickness) is formed. The dark region in the TEM image is a Au nanocap and the bright region is a β-$NaYF_4$ nanorod. From the HAADF image, we can see that the nanocap covers the upper part of the nanorod. The surface of the Au nanocap is very smooth. TEM images of other samples with different aspect ratios are shown in Figure 5i and k together with the schematic illustrations (Figure 5j and l, respectively).

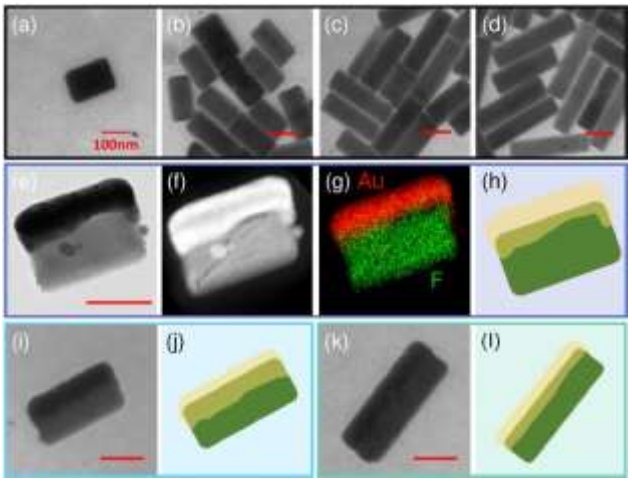


**Figure 5.** (a-d) TEM images of β-$NaYF_4$:Er/Yb nanorods with different aspect ratios. The dimensions estimated from TEM images are 100 × 150 nm (aspect ratio 1.5) (a), 100 × 200 nm (aspect ratio 2) (b), 75 × 230 nm (aspect ratio 3) (c) and 50 × 200 nm (aspect ratio 4) (d). (e-g) TEM image (e), HAADF-STEM image (f), EDS mapping image (Au and F) (g), and schematic

illustration (h) of a β-$NaYF_4$:Er/Yb nanorod (105 × 177 nm) with a Au nanocap (30 nm in thickness). (i, j) TEM image and schematic illustration of a β-$NaYF_4$:Er/Yb nanorod (100 × 220 nm) with a Au nanocap (20 nm in thickness). (k, l) TEM image and schematic illustration of a β-$NaYF_4$:Er/Yb nanorod (95 × 300 nm) with a Au nanocap (20 nm in thickness).

Figure 6a shows the scattering spectrum of the nanorod in Figure 5k (aspect ratio ~3). It has two peaks at 697 nm and 979 nm. The spectral feature is very similar to the calculated extinction cross section spectra in Figures 1 and 2, although the intensity ratio is different. As mentioned above, for the scattering measurements, a high numerical aperture objective is used. In this setup, all resonance modes including ED, MD (S) and MD (L) can be excited regardless of the orientation of nanorods. However, the intensity ratio depends on the nanorod orientation and it is not controlled in this work. Therefore, we do not discuss the spectral shape and focus only on the peak wavelengths. In some nanorods, we observed only one peak. This is either due to the overlap of two peaks because of the small separation or due to very small intensity of one of the peaks. In the former case, the peak can be separated by a polarization-resolved scattering measurement (Figure S2 in the Supporting Information).

We measured the scattering spectra for many isolated nanorods. The spectra and corresponding TEM images are shown in the Supporting Information (Figure S3). The peak wavelengths obtained from the spectra are plotted in Figure 6(b-d). In these graphs, the abscissa is the wavelength, and the ordinate is the length of the long axis. The length of the short axis is 100, 75 and 50 nm for Figure 6b, c and d, respectively. The nanocap thickness is 30 nm in Figure 6b, and is 20 nm in Figure 6c and d. If we observe two peaks clearly in a spectrum, the short wavelength one is plotted with a blue triangle, while the long wavelength one is plotted with a black triangle. If only one

peak is observed, it is plotted with a green square symbol. In the figures, scattering cross sections obtained by simulations are also shown by color gradients. We can see relatively good agreement between the wavelengths of scattering peaks and scattering cross sections. The agreement indicates that the observed scattering peaks are MD (S) and MD (L) modes of Au nanocaps. The small difference between experiments and calculations may arise from structural imperfection of synthesized nanorods such as the variation of nanocap shape.

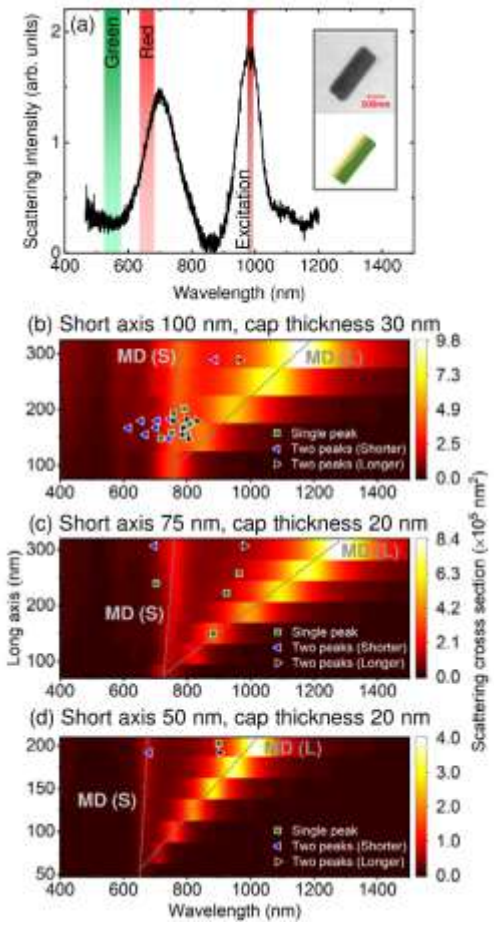


**Figure 6.** (a) Scattering spectrum of a β-$NaYF_4$:Er/Yb nanorod (95 × 300 nm) with an Au nanocap (20 nm in thickness). Insets are the TEM image and the illustration. (b-d) Color maps of calculated scattering cross section as a function of wavelength (abscissa) and long axis length (ordinate). The

short axis length is (b) 100 nm, (c) 75 nm and (d) 50 nm. The Au nanocap thickness is (b) 30 nm and (c, d) 20 nm. On the graphs, peaks in measured scattering spectra are shown by symbols. In the case of spectra with two peaks, the short wavelength one is plotted with a blue triangle, while the long wavelength one is plotted with a black triangle. In the case of spectra with one peak, it is plotted with a green square symbol.

Figure 7a shows an upconversion spectrum of the nanorod in Figure 5k (aspect ratio ~3) (red). An upconversion spectrum of a β-$NaYF_4$ nanorod without a Au nanocap is also shown as a reference (black). The nanorod without a Au nanocap is prepared by exactly the same procedure as that with a Au nanocap, *i.e.*, a Au nanocap is accidentally removed from it during the ultrasonication process. Therefore, both nanorods experienced the same thermal history. This is very important to compare the upconversion intensity and extract the effect of an Au nanocap because upconversion efficiency of a β-$NaYF_4$:Er/Yb nanorod is very sensitive to the thermal history. The green (~550 nm) and red (~660 nm) emission bands correspond to the $^4S_{3/2}$ and $^4F_{9/2}$, respectively, to $^4I_{15/2}$ transition in the 4*f* state of $Er^{3+}$ ions. We can see strong enhancement of the upconversion intensity by the formation of the nanocap.

In Figure 7b, the intensities of the green and red emissions of β-$NaYF_4$:Er/Yb nanorods with Au nanocaps divided by those of a β-$NaYF_4$:Er/Yb nanorod without a Au nanocap (the sample in the inset of Figure 6a) are plotted as a function of the wavelength of the scattering peak. In the case of a nanorod with multiple scattering peaks, the longest wavelength one is adopted. Note that, within the present work, it is not possible to quantitatively estimate the enhancement factor because the reference β-$NaYF_4$:Er/Yb nanorod without an Au nanocap is chosen randomly. Therefore, the ordinate of Figure 7b is arbitrary units. We can see clear correlation between the resonance

wavelength and the enhancement factor; it increases rapidly as the resonance wavelength approaches the excitation wavelength of upconversion (980 nm). The clear correlation indicates that the observed upconversion enhancement is predominantly due to the coupling with the plasmonic modes of elongated Au nanocaps, although a small fraction of the observed trend (at most factor of 6) is due to nanorod length (volume) increase from left to right in Figure 7b.

In general, Au nanocap affects the excitation process, energy transfer process, relaxation process and emission process of upconversion of a β-$NaYF_4$:Er/Yb nanorod.[48–50] The strong increase of the upconversion intensity as the resonance wavelength approaches the excitation wavelength indicates that the enhancements of the excitation field and/or the energy transfer rate are the dominant factor for the upconversion enhancement. Although it is not easy to experimentally distinguish these mechanisms, given the relatively weak excitation intensity (1.1 kW/$cm^2$), the former would be dominant. Concerning the emission process, we estimated by numerical simulations that the antenna efficiency of a nanocap is ~30%, which is larger than the quantum yield of $Er^{3+}$ and $Yb^{3+}$ doped β-$NaYF_4$ generally reported (~1%).[44,45] Therefore, the Purcell enhancement may also contribute to the upconversion enhancement. Further studies especially the decay rate measurements of single nanorods are necessary for the quantitative discussion of the Purcell enhancement.[48]

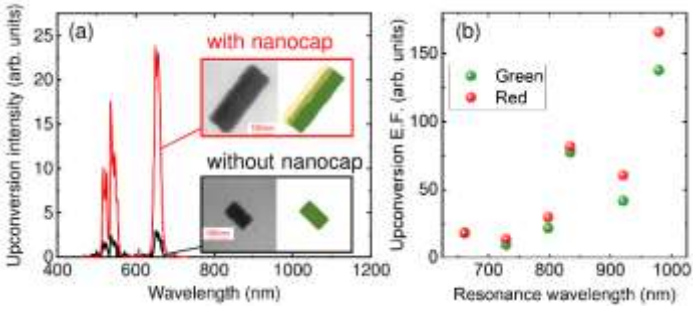

**Figure 7.** (a) Upconversion spectrum of a β-$NaYF_4$:Er/Yb nanorod (95 × 300 nm) with a Au nanocap (20 nm in thickness) (red). An upconversion spectrum of a β-$NaYF_4$ nanorod without a Au nanocap is shown as a reference (black). Insets are the TEM images and the illustrations. (b) Green and red upconversion enhancement factor as a function of the resonance wavelength of the nanocap. In the case of a nanorod with multiple scattering peaks, the longest wavelength one is adopted.

## CONCLUSION

We proposed an elongated metal nanocap as a component of a stand-alone plasmonic nanocomposite. We first showed by numerical simulation that two MD modes exist in an elongated metal nanocap and the resonance wavelengths can be controlled in a wide range. We then fabricated β-$NaYF_4$:Er/Yb nanorods with Au nanocaps and performed the comprehensive structural characterizations. The scattering spectra of individual nanocomposites revealed that the designed structure can be successfully produced and the resonance wavelength can be controlled in a wide range. Finally, we studied upconversion of β-$NaYF_4$:Er/Yb nanorods with Au nanocaps and found that tuning the resonance wavelength of the Au nanocap to the excitation wavelength results in the significant enhancement. To the best of our knowledge, this is the first report for the fabrication of an elongated metal nanocap and the study of the plasmonic property. Because of the high degree of freedom to tune the resonance wavelengths, this structure can be used for the enhancement of a variety of optical phenomena such as Raman scattering, second/third harmonic generations, etc.

ASSOCIATED CONTENT

**Supporting Information**.

The following files are available free of charge.

TEM images of various nanocomposites not used in this work, polarization-resolved scattering measurement of single nanocomposites, details of β-$NaYF_4$:Er,Yb nanorod synthesis process, and scattering spectra and TEM images of single β-$NaYF_4$:Er/Yb nanorods with Au nanocaps (PDF)

AUTHOR INFORMATION

**Corresponding Author**

*fujii@eedept.kobe-u.ac.jp

**Notes**

The authors declare no competing financial interest.

ACKNOWLEDGMENT

T.H.'s work acknowledges support from Grant-in-Aid for JSPS Research Fellows. This work was partly supported by JSPS KAKENHI Grant Number 16H03828, 18K14092, and 18J20276.

REFERENCES

(1) Ming, T.; Chen, H.; Jiang, R.; Li, Q.; Wang, J. Plasmon-Controlled Fluorescence: Beyond the Intensity Enhancement. *J. Phys. Chem. Lett.* **2012**, *3*, 191–202.

(2) Hayashi, S.; Okamoto, T. Plasmonics: Visit the Past to Know the Future. *J. Phys. D. Appl. Phys.* **2012**, *45*, 433001.

(3) Giannini, V.; Fernández-Domínguez, A. I.; Heck, S. C.; Maier, S. A. Plasmonic Nanoantennas: Fundamentals and Their Use in Controlling the Radiative Properties of Nanoemitters. *Chem. Rev.* **2011**, *111*, 3888–3912.

(4) Koenderink, A. F. Single-Photon Nanoantennas. *ACS Photonics* **2017**, *4*, 710–722.

(5) Lakowicz, J. R.; Ray, K.; Chowdhury, M.; Szmacinski, H.; Fu, Y.; Zhang, J.; Nowaczyk, K. Plasmon-Controlled Fluorescence: A New Paradigm in Fluorescence Spectroscopy. *Analyst* **2008**, *133*, 1308–1346.

(6) Sugimoto, H.; Chen, T.; Wang, R.; Fujii, M.; Reinhard, B. M.; Dal Negro, L. Plasmon-Enhanced Emission Rate of Silicon Nanocrystals in Gold Nanorod Composites. *ACS Photonics* **2015**, *2*, 1298–1305.

(7) Benz, F.; Schmidt, M. K.; Dreismann, A.; Chikkaraddy, R.; Zhang, Y.; Demetriadou, A.; Carnegie, C.; Ohadi, H.; de Nijs, B.; Esteban, R.; et al. Single-Molecule Optomechanics in "Picocavities." *Science* **2016**, *354*, 726–729.

(8) Curto, A. G.; Volpe, G.; Taminiau, T. H.; Kreuzer, M. P.; Quidant, R.; van Hulst, N. F. Unidirectional Emission of a Quantum Dot Coupled to a Nanoantenna. *Science* **2010**, *329*, 930–933.

(9) Zhang, J.; Fu, Y.; Chowdhury, M. H.; Lakowicz, J. R. Single-Molecule Studies on Fluorescently Labeled Silver Particles: Effects of Particle Size. *J. Phys. Chem. C* **2008**, *112*, 18–26.

(10) Ge, W.; Zhang, X. R.; Liu, M.; Lei, Z. W.; Knize, R. J.; Lu, Y. Distance Dependence of Gold-Enhanced Upconversion Luminescence in Au/SiO2/Y2O3 :Yb3+, Er3+ Nanoparticles. *Theranostics* **2013**, *3*, 282–288.

(11) Inoue, A.; Sugimoto, H.; Yaku, H.; Fujii, M. DNA Assembly of Silicon Quantum Dots/Gold Nanoparticle Nanocomposites. *RSC Adv.* **2016**, *6*, 63933–63939.

(12) Inoue, A.; Fujii, M.; Sugimoto, H.; Imakita, K. Surface Plasmon-Enhanced Luminescence of Silicon Quantum Dots in Gold Nanoparticle Composites. *J. Phys. Chem. C* **2015**, *119*, 25108–25113.

(13) Song, Y.; Liu, G.; Dong, X.; Wang, J.; Yu, W.; Li, J. Au Nanorods@NaGdF4/Yb3+ ,Er3+ Multifunctional Hybrid Nanocomposites with Upconversion Luminescence, Magnetism, and Photothermal Property. *J. Phys. Chem. C* **2015**, *119*, 18527–18536.

(14) Huang, Y.; Rosei, F.; Vetrone, F. A Single Multifunctional Nanoplatform Based on Upconversion Luminescence and Gold Nanorods. *Nanoscale* **2015**, *7*, 5178–5185.

(15) Kang, F.; He, J.; Sun, T.; Bao, Z. Y.; Wang, F.; Lei, D. Y. Plasmonic Dual-Enhancement and Precise Color Tuning of Gold Nanorod@SiO2 Coupled Core-Shell-Shell Upconversion Nanocrystals. *Adv. Funct. Mater.* **2017**, 1701842.

(16) Li, H.; Deng, Q.; Liu, B.; Yang, J.; Wu, B. Fabrication of Core@spacer@shell Au Nanorod @mSiO2@Y2O3:Er Nanocomposites with Enhanced Upconversion Fluorescence. *RSC Adv.* **2016**, *6*, 13343–13348.

(17) He, J.; Zheng, W.; Ligmajer, F.; Chan, C.-F.; Bao, Z.; Wong, K.-L.; Chen, X.; Hao, J.; Dai, J.; Yu, S.-F.; et al. Plasmonic Enhancement and Polarization Dependence of

Nonlinear Upconversion Emissions from Single Gold Nanorod@SiO2@CaF2:Yb3+,Er3+ Hybrid Core–Shell–Satellite Nanostructures. *Light Sci. Appl.* **2017**, *6*, e16217.

(18) Zhang, J.; Gryczynski, I.; Gryczynski, Z.; Lakowicz, J. R. Dye-Labeled Silver Nanoshell−Bright Particle. *J. Phys. Chem. B* **2006**, *110*, 8986–8991.

(19) Fujii, M.; Nakano, T.; Imakita, K.; Hayashi, S. Upconversion Luminescence of Er and Yb Codoped NaYF 4 Nanoparticles with Metal Shells. *J. Phys. Chem. C* **2013**, *117*, 1113–1120.

(20) Ayala-Orozco, C.; Liu, J. G.; Knight, M. W.; Wang, Y.; Day, J. K.; Nordlander, P.; Halas, N. J. Fluorescence Enhancement of Molecules Inside a Gold Nanomatryoshka. *Nano Lett.* **2014**, *14*, 2926–2933.

(21) Khlebtsov, B.; Khanadeev, V.; Khlebtsov, N. Surface-Enhanced Raman Scattering inside Au@Ag Core/Shell Nanorods. *Nano Res.* **2016**, *9*, 2303–2318.

(22) Hinman, J. G.; Stork, A. J.; Varnell, J. A.; Gewirth, A. A.; Murphy, C. J. Seed Mediated Growth of Gold Nanorods: Towards Nanorod Matryoshkas. *Faraday Discuss.* **2016**, *191*, 9–33.

(23) Yamamoto, K.; Fujii, M.; Sowa, S.; Imakita, K.; Aoki, K. Upconversion Luminescence of Rare-Earth-Doped Y2O3 Nanoparticle with Metal Nano-Cap. *J. Phys. Chem. C* **2015**, *119*, 1175–1179.

(24) Hinamoto, T.; Takashina, H.; Sugimoto, H.; Fujii, M. Controlling Surface Plasmon Resonance of Metal Nanocap for Upconversion Enhancement. *J. Phys. Chem. C* **2017**, *121*, 8077–8083.

(25) Bang, D.; Jo, E.-J.; Hong, S.; Byun, J.-Y.; Lee, J. Y.; Kim, M.-G.; Lee, L. P. Asymmetric Nanocrescent Antenna on Upconversion Nanocrystal. *Nano Lett.* **2017**, *17*, 6583–6590.

(26) Hinamoto, T.; Sugimoto, H.; Fujii, M. Metal-Core/Dielectric-Shell/Metal-Cap Composite Nanoparticle for Upconversion Enhancement. *J. Phys. Chem. C* **2018**, *122*, 17465–17472.

(27) Ringler, M.; Schwemer, A.; Wunderlich, M.; Nichtl, A.; Kürzinger, K.; Klar, T. A.; Feldmann, J. Shaping Emission Spectra of Fluorescent Molecules with Single Plasmonic Nanoresonators. *Phys. Rev. Lett.* **2008**, *100*, 203002.

(28) Bidault, S.; Devilez, A.; Maillard, V.; Lermusiaux, L.; Guigner, J.-M.; Bonod, N.; Wenger, J. Picosecond Lifetimes with High Quantum Yields from Single-Photon-Emitting Colloidal Nanostructures at Room Temperature. *ACS Nano* **2016**, *10*, 4806–4815.

(29) Das, A.; Mao, C.; Cho, S.; Kim, K.; Park, W. Over 1000-Fold Enhancement of Upconversion Luminescence Using Water-Dispersible Metal-Insulator-Metal Nanostructures. *Nat. Commun.* **2018**, *9*, 4828.

(30) Qin, Y.; Dong, Z.; Zhou, D.; Yang, Y.; Xu, X.; Qiu, J. Modification on Populating Paths of β-NaYF4:Nd/Yb/Ho@SiO2@Ag Core/Double-Shell Nanocomposites with Plasmon Enhanced Upconversion Emission. *Opt. Mater. Express* **2016**, *6*, 1942–1955.

(31) Liu, S.; Chen, G.; Ohulchanskyy, T. Y.; Swihart, M. T.; Prasad, P. N. Facile Synthesis and Potential Bioimaging Applications of Hybrid Upconverting and Plasmonic NaGdF 4 : Yb 3+ , Er 3+ /Silica/Gold Nanoparticles. *Theranostics* **2013**, *3*, 275–281.

(32) Kannan, P.; Abdul Rahim, F.; Chen, R.; Teng, X.; Huang, L.; Sun, H.; Kim, D.-H. Au Nanorod Decoration on NaYF 4 :Yb/Tm Nanoparticles for Enhanced Emission and

Wavelength-Dependent Biomolecular Sensing. *ACS Appl. Mater. Interfaces* **2013**, *5*, 3508–3513.

(33) Lassiter, J. B.; Knight, M. W.; Mirin, N. A.; Halas, N. J. Reshaping the Plasmonic Properties of an Individual Nanoparticle. *Nano Lett.* **2009**, *9*, 4326–4332.

(34) King, N. S.; Li, Y.; Ayala-Orozco, C.; Brannan, T.; Nordlander, P.; Halas, N. J. Angle- and Spectral-Dependent Light Scattering from Plasmonic Nanocups. *ACS Nano* **2011**, *5*, 7254–7262.

(35) Mirin, N. A.; Halas, N. J. Light-Bending Nanoparticles. *Nano Lett.* **2009**, *9*, 1255–1259.

(36) Zhang, Y.; Barhoumi, A.; Lassiter, J. B.; Halas, N. J. Orientation-Preserving Transfer and Directional Light Scattering from Individual Light-Bending Nanoparticles. *Nano Lett.* **2011**, *11*, 1838–1844.

(37) King, N. S.; Knight, M. W.; Large, N.; Goodman, A. M.; Nordlander, P.; Halas, N. J. Orienting Nanoantennas in Three Dimensions To Control Light Scattering Across a Dielectric Interface. *Nano Lett.* **2013**, *13*, 5997–6001.

(38) García de Abajo, F. J. Multiple Scattering of Radiation in Clusters of Dielectrics. *Phys. Rev. B* **1999**, *60*, 6086–6102.

(39) Hohenester, U.; Trügler, A. MNPBEM – A Matlab Toolbox for the Simulation of Plasmonic Nanoparticles. *Comput. Phys. Commun.* **2012**, *183*, 370–381.

(40) Geuzaine, C.; Remacle, J.-F. Gmsh: A 3-D Finite Element Mesh Generator with Built-in Pre- and Post-Processing Facilities. *Int. J. Numer. Methods Eng.* **2009**, *79*, 1309–1331.

(41) Johnson, P. B.; Christy, R. W. Optical Constants of the Noble Metals. *Phys. Rev. B* **1972**, *6*, 4370–4379.

(42) Lu, G.; Zhang, T.; Li, W.; Hou, L.; Liu, J.; Gong, Q. Single-Molecule Spontaneous Emission in the Vicinity of an Individual Gold Nanorod. *J. Phys. Chem. C* **2011**, *115*, 15822–15828.

(43) Novotny, L.; van Hulst, N. Antennas for Light. *Nat. Photonics* **2011**, *5*, 83–90.

(44) Kaiser, M.; Würth, C.; Kraft, M.; Hyppänen, I.; Soukka, T.; Resch-Genger, U. Power-Dependent Upconversion Quantum Yield of NaYF4:Yb3+ ,Er3+ Nano- and Micrometer-Sized Particles – Measurements and Simulations. *Nanoscale* **2017**, *9*, 10051–10058.

(45) Boyer, J.-C.; van Veggel, F. C. J. M. Absolute Quantum Yield Measurements of Colloidal NaYF4: Er3+, Yb3+ Upconverting Nanoparticles. *Nanoscale* **2010**, *2*, 1417–1419.

(46) Wang, F.; Liu, X. Recent Advances in the Chemistry of Lanthanide-Doped Upconversion Nanocrystals. *Chem. Soc. Rev.* **2009**, *38*, 976.

(47) Wang, F.; Han, Y.; Lim, C. S.; Lu, Y.; Wang, J.; Xu, J.; Chen, H.; Zhang, C.; Hong, M.; Liu, X. Simultaneous Phase and Size Control of Upconversion Nanocrystals through Lanthanide Doping. *Nature* **2010**, *463*, 1061–1065.

(48) Lu, D.; Cho, S. K.; Ahn, S.; Brun, L.; Summers, C. J.; Park, W. Plasmon Enhancement Mechanism for the Upconversion Processes in NaYF4:Yb3+,Er3+ Nanoparticles: Maxwell versus Förster. *ACS Nano* **2014**, *8*, 7780–7792.

(49) Maier, S. A. *Plasmonics: Fundamentals and Applications*; Springer US: New York, NY, 2007.

(50) Pavani, K.; Suresh Kumar, J.; Srikanth, K.; Soares, M. J.; Pereira, E.; Neves, A. J.; Graça, M. P. F. Highly Efficient Upconversion of Er3+ in Yb3+ Codoped Non-Cytotoxic Strontium Lanthanum Aluminate Phosphor for Low Temperature Sensors. *Sci. Rep.* **2017**, *7*, 17646.

TOC Graphic